

Self-consistent radiative effect on relativistic electromagnetic particle acceleration

K. NOGUCHI⁽¹⁾, E. LIANG⁽¹⁾, K. NISHIMURA⁽²⁾

⁽¹⁾ *Dept. of Physics and Astronomy, Rice Univ., Houston TX, USA*

⁽²⁾ *AdvanceSoft, Tokyo Japan*

Summary.— We study the radiation damping effect on the relativistic acceleration of electron-positron plasmas with two-and-half-dimensional particle-in-cell (PIC) simulation. Particles are accelerated by Poynting flux via the diamagnetic relativistic pulse accelerator (DRPA), and decelerated by the self-consistently solved radiation damping force. With $\Omega_{ce}/\omega_{pe} \geq 10$, the Lorentz factor of the highest energy particles reaches $\gamma > 100$, and the acceleration still continues. The emitted radiation is peaked within few degrees from the direction of Poynting flux and strongly linearly polarized, which may be detectable in γ -ray burst (GRB) observations. We also show that the DRPA is insensitive to the initial supporting currents.

PACS 52.65.-y – Plasma simulation.

PACS 52.65.Rr – Particle-in-cell method.

PACS 52.30.-q – Plasma dynamics and flow.

One of the unsolved problems in astrophysics is the acceleration of nonthermal high-energy particles, whose radiation is observed from pulsars, blazars, gamma-ray bursts and black holes. Recently, a new mechanism of relativistic nonthermal particle acceleration, called the Diamagnetic Relativistic Pulse Accelerator (DRPA), was discovered using multi-dimensional Particle-in-Cell (PIC) simulations. When a plasma-loaded electromagnetic pulse expands relativistically, the self-induced drift current creates ponderomotive trap, which drags only the fast particles in the trap and leave slow ones behind. At late times the DRPA reproduces many of the unique signatures of GRBs, including time profiles, spectra and spectral evolution [1].

When charged particles suffer extreme acceleration, radiation loss and damping can become important in the plasma energetics and dynamics. However, conventional Particle-in-Cell (PIC) simulations of collisionless plasmas have not included radiation effects. In this article we report PIC simulation results using a newly developed 2-1/2-D code that includes self-consistent radiation damping.

In PIC simulations, it is impractical to include high-frequency radiation into the electromagnetic field calculation because the radiation wavelength is much shorter than the spatial resolution of the fields (\sim Debye length $\lambda_D \equiv c/\omega_{pe}$, where $\omega_{pe} = \sqrt{4\pi\rho e/m_e}$ is the electron plasma frequency). Accelerated particles can emit up to the critical

frequency $\omega_c = 3\gamma^2\Omega_{ce}$, where $\gamma = E/m_ec^2 = 1/\sqrt{1-v^2/c^2}$ and $\Omega_{ce} = eB/(m_ec)$ is the electron gyro-frequency. The ratio of the critical radiation wavelength λ_c to λ_D is given by $\lambda_c/\lambda_D = (2\pi\omega_{pe})/(3\gamma^3\Omega_{ce})$, which is $\ll 1$ because $\omega_{pe}/\Omega_{ce} < 0.1$ in magnetic-dominated cases and $\gamma \gg 1$.

Instead of calculating the high-frequency component directly, we introduce a radiation damping force in the form of the Dirac-Lorentz equation [3]. The relativistic damping force term \mathbf{f}_{rad} is given by (see [3] for detailed calculations)

$$(1) \quad \mathbf{f}_{rad} = \frac{2e}{3\Omega_{ce}} k_{rad} \left\{ \gamma \left[\left(\frac{\partial}{\partial t} + \mathbf{v} \cdot \nabla \right) \mathbf{E} + \frac{\mathbf{v}}{c} \times \left(\frac{\partial}{\partial t} + \mathbf{v} \cdot \nabla \right) \mathbf{B} \right] + \frac{e}{mc} \left[\mathbf{E} \times \mathbf{B} \right. \right. \\ \left. \left. + \frac{1}{c} \mathbf{B} \times (\mathbf{B} \times \mathbf{v}) + \frac{1}{c} \mathbf{E} (\mathbf{v} \cdot \mathbf{E}) \right] - \frac{e\gamma^2}{mc^2} \mathbf{v} \left[\left(\mathbf{E} + \frac{1}{c} \mathbf{v} \times \mathbf{B} \right)^2 - \frac{1}{c^2} (\mathbf{E} \cdot \mathbf{v})^2 \right] \right\},$$

where \mathbf{v} is the velocity, and \mathbf{E} and \mathbf{B} are the self-consistent electric and magnetic fields. Here we introduce a non-dimensional factor k_{rad} given by

$$(2) \quad k_{rad} = \frac{r_e \Omega_{ce}}{c} = 1.64 \times 10^{-16} \times B(\text{gauss}),$$

where $r_e = e^2/(mc^2)$ is the classical electron radius. The first square bracket term of the radiation damping force (1) represents the radiation damping due to the ponderomotive force acceleration. The third square bracket term is Compton scattering by large scale ($\lambda > \lambda_D$) electromagnetic field which reduces to Thomson scattering in the classical limit [5]. We should note here that the scattering between high frequency radiation and particles is not considered since all fields are averaged over Debye length.

The power spectrum analysis [1] shows that our simulation model with $\omega_{pe}/\Omega_{ce} = 10$ corresponds to the GRBs with initial magnetic energy $\sim 10^{51}$ ergs by assuming a 4π shell of thickness 10^{12} cm and radius 10^{13} cm. If GRBs are originated from a region $< 10^8$ cm, this magnetic energy implies an initial $B > 10^{13}$ G, which corresponds to $k_{rad} \sim 10^{-3}$.

We should restrict ourselves not to reach the quantum-limit, $\hbar\Omega_{ce} \sim m_ec^2$ or $B > 4.4 \times 10^{13}$ G, which corresponds to $k_{rad} = 7.2 \times 10^{-3}$, or the formula (1) fails. We choose k_{rad} from zero to 10^{-3} in the simulation to enhance the radiation effect and $|\mathbf{f}_{rad}| \tau_{sim} \simeq |\mathbf{F}_{ext}| \Omega_{ce}^{-1}$ so we can see the difference between radiative and non-radiative ($k_{rad} = 0$) case within the simulation time-scale $\tau_{sim} = O(10^4 \Omega_{ce}^{-1})$.

We use the 2-1/2D explicit PIC simulation scheme using the explicit leap-frogging method for time advancing [6]. Spatial grids for the fields are uniform in both x and z directions, $\Delta x = \Delta z = \lambda_D$. The simulation domain in the $x-z$ plane is $-L_x/2 \leq x \leq L_x/2$ and $0 \leq z \leq L_z$ with a doubly periodic boundary condition in both directions.

Following Liang et. al. [1], the initial plasma is uniformly distributed at the center of the simulation box, $-6\Delta x < x < 6\Delta x$ and $0 < z < L_z$. The background uniform magnetic field $\mathbf{B}_0 = (0, B_0, 0)$ is applied only in the same region, so that the magnetic field freely expands toward the vacuum regions, $x > 6\Delta x$ and $x < -6\Delta x$ with accelerating plasma. We choose L_x to be long enough so that plasma and EM wave never hit the boundaries in the x direction within the simulation time. The initial temperature of plasma is assumed to be a spatially uniform relativistic Maxwellian, $k_B T_e = k_B T_p = 1\text{MeV}$, where the subscripts e and p refer to electrons and positrons.

Since its discovery, questions have been asked if DRPA would persist if the initial static \mathbf{B} field is confined by supporting currents ($\mathbf{J} = \nabla \times \mathbf{B}$), instead of being simply

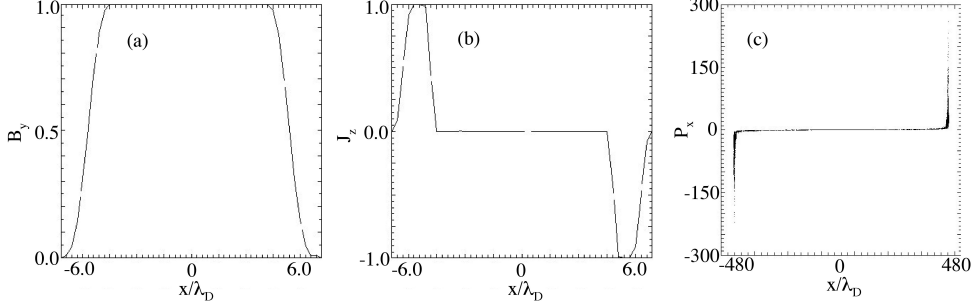


Fig. 1. – An example of the DRPA with initial current $\mathbf{J} = \nabla \times \mathbf{B}$, $\omega_{pe}/\Omega_{ce} = 0.1$, $k_{rad} = 0$. The initial magnetic field and current distribution are shown in panels (a) and (b). The phase plot of particles at $t\Omega_{ce} = 4800$ is shown in panel (c).

superposition of opposite traveling waves with initial $\mathbf{J} = 0$. Figure 1 shows an example of a PIC simulation with initial current distribution $\mathbf{J} = \nabla \times \mathbf{B}$. We use a finer grid $\Delta x = \lambda_D/3$ in this case to resolve the gradient of fields near the plasma surface. At $t = 0$, magnetic field is smoothly decreased toward the edge $x/\lambda_D = \pm 6$, and initial current is locally distributed near the edges. However, the initial current is rapidly dissipated by the expanding plasma, and two EM pulses are formed as in the case without initial current. The asymptotic phase plot is shown in Fig. 1 (c). It is basically identical to the DRPA phase plot without initial \mathbf{J} .

We choose six different sets of parameters shown in Table I for the radiative calculations, by changing $k_{rad} = 0, 10^{-4}, 10^{-3}$ and $\omega_{pe}/\Omega_{ce} = 0.1, 0.01$, and run simulations for each case.

Figure 2 shows the momentum distribution of particles for (a) Run A($x < 0$) and Run C($x > 0$), and (b) Run D($x < 0$) and Run F($x > 0$). The DRPA accelerates electrons and positrons in the same direction along the x axis, whereas electric field accelerates electrons and positrons oppositely along the z axis, forming X shape distribution in the $p_x - p_z$ plane as a result. Resulted induced current J_z accelerates particles in the x direction by the ponderomotive force $\mathbf{J} \times \mathbf{B}$. The ponderomotive force creates successive ‘potential wells’ in the x direction, which captures and accelerates co-moving particles. We emphasize here that there is no charge separation in the x direction because there is no mass difference between electron and positron.

Obviously, particle momenta in both x and z directions are radiated away in both weak

TABLE I. – *The parameters for radiative runs*

	k	ω_{pe}/Ω_{ce}	Duration $t\Omega_{ce}$
Run A	0	0.1	10000
Run B	10^{-4}	0.1	10000
Run C	10^{-3}	0.1	10000
Run D	0	0.01	70000
Run E	10^{-4}	0.01	70000
Run F	10^{-3}	0.01	70000

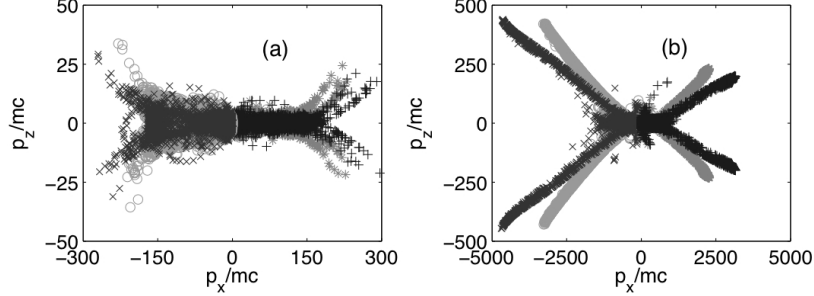


Fig. 2. – Momentum distribution of particles for Run A [(a), $x < 0$] and Run C [(a), $x > 0$] at $t\Omega_{ce} = 5000$ (circle, asterisk) and $t\Omega_{ce} = 10000$ (cross, plus), and Run D [(b), $x < 0$] and Run F [(b), $x > 0$] at $t\Omega_{ce} = 35000$ (circle, asterisk) and $t\Omega_{ce} = 70000$ (cross, plus). Results in the positive and negative x directions are identical in all cases.

and strong magnetic field RD cases. For high energy ($\gamma \gg 1$) particles, the Compton scattering [the third term in Eq. (1)] becomes dominant damping force, and makes the DRPA acceleration less efficient.

With radiation damping, we can calculate the self-consistent radiation field and its angular dependence directly from the velocity and acceleration of each particle. Intensity I and polarization Π of the radiation received by the observer located at \mathbf{x} are given by [4, 5]

$$(3) \quad I(\hat{\mathbf{n}}, \tau) = \sum_i \left[|\mathbf{E}_i|^2 \right]_{\text{ret}}, \quad \Pi(\hat{\mathbf{n}}, \tau) = \frac{\sqrt{(E_z^2)^2 + (E_y^2)^2 - 2E_y^2E_z^2 + U^2}}{E_z^2 + E_y^2},$$

where

$$(4) \quad \begin{aligned} E_y^2(\hat{\mathbf{n}}, \tau) &= \sum_i \left[|\mathbf{E}_i \cdot \hat{\mathbf{y}}|^2 \right]_{\text{ret}}, & E_z^2(\hat{\mathbf{n}}, \tau) &= \sum_i \left[|\mathbf{E}_i \cdot \hat{\mathbf{z}}|^2 \right]_{\text{ret}}, \\ U(\hat{\mathbf{n}}, \tau) &= 2 \sum_i [(\mathbf{E}_i \cdot \hat{\mathbf{y}})(\mathbf{E}_i \cdot \hat{\mathbf{z}})]_{\text{ret}}, & \mathbf{E}_i &= \frac{e \hat{\mathbf{n}} \times [(\hat{\mathbf{n}} - \hat{\beta}_i) \times \dot{\beta}_i]}{c (1 - \hat{\mathbf{n}} \cdot \hat{\beta})^3 R}, \end{aligned}$$

where the sum is over all particles along each light cone. $\hat{\mathbf{n}}$ is a unit vector in the direction of $\mathbf{x} - \mathbf{r}(\tau)$, $\hat{\beta} = \mathbf{v}(\tau)/c$, and $\dot{\beta} = d\beta/dt$. We assume that $|\mathbf{x}| \gg |\mathbf{r}|$ so that $\hat{\mathbf{n}}$ is parallel to \mathbf{x} . The square brackets with a subscript "ret" mean that the quantity in the brackets is evaluated at the retarded time $\tau = t - R/c$, where $R = |\mathbf{x} - \mathbf{r}|$. To specify the direction of the observer with respect to the x axis, we introduce θ and ϕ as $\hat{\mathbf{n}} = (\cos \theta \cos \phi, \cos \theta \sin \phi, \sin \theta)$.

In Figs. 3(a) and (b), the contour plot of instantaneous intensity before taking the summation over the retarded time is plotted, as a function of local time t with $\phi = \theta = 0$, illustrating the ray-tracing technique used in Eqs. (3) and (4). We take a sum of intensity along the light cone $\tau = t - R/c = \text{const.}$, which is indicated as a solid line in the panel (a), up to $t\Omega_{ce} = 10000$ for Run C and $t\Omega_{ce} = 70000$ for Run F. The light cone moves up in t with increasing τ , and we take $\tau = 0$ when the pulse front reaches to the observer.

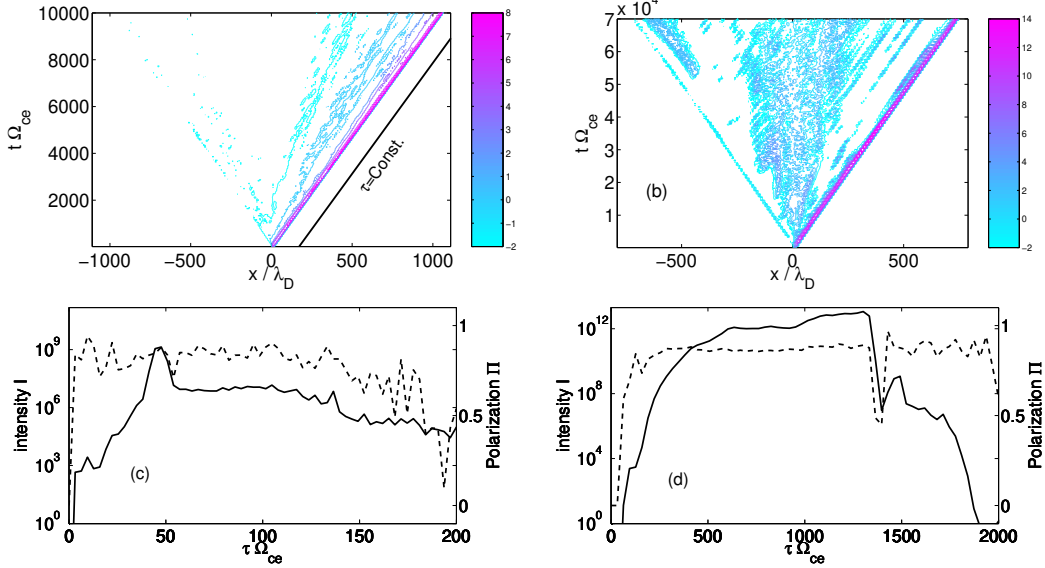


Fig. 3. – Contour plots of instantaneous intensity $\log_{10} I$ per particle as a function of local time t for $\theta = \phi = 0$ for (a) Run C and (b) Run F. Total detected intensity (solid lines, right scales) and polarization (dashed lines, left scales) as functions of observational time τ for (c) Run C and (d) Run F. Intensity is in arbitrary scale. To obtain time dependence of intensity, instantaneous intensity from each particle is summed up along the light cone $\tau = t - R/c = \text{const.}$, shown as a black line in panel (a). The light cone moves horizontally leftward with τ .

We also note that the intensity is extremely asymmetric because only energetic particles accelerated in positive x direction can radiate strong emission to the observer.

The time dependence of detected intensity and the polarization with $\phi = \theta = 0$ are shown in Figs. 3(c) and (d). Energetic particles are bouncing back and forth within the ponderomotive potential well, and slower particles are dropped off to the next well, which broaden the spatial distribution and the resulting radiation duration.

Intensity I is shown as solid lines in Fig. 3(b) and (d), indicating the duration time of strong intensity radiation is $20\tau\Omega_{ce}$ for Run C, and $200 \sim 400\tau\Omega_{ce}$ for Run D with single peak. Since the driving electromagnetic field is linearly polarized, we expect that the radiation is strongly polarized with the small depolarization coming from the initial random y velocity. Dotted lines in Fig. 3(b) and (d) shows that the radiation is strongly linear-polarized as anticipated.

In Fig. 4, we show the total radiation intensity $\int I(\phi, \theta) d\tau$. The radiation is a very short pulse in Fig. 3 because we consider single simulation box centered at the origin only. However, because of the periodic boundary condition in the z direction, we should consider the multiple simulation boxes along the z axis, and consider time delay and angle difference toward the observer from each simulation box, which is very complex even in the Cartesian coordinate.

Instead of including these geometrical effects into the intensity calculation, we simply compare the total fluence integrated over t as a function of the angle. Angular fluence peaks around $\theta = 3 \sim 8^\circ$ in $\phi = 0$ cases (solid and dash-dot lines), corresponding to the direction of high energy particles in Fig. 2. Angular fluence rapidly decreases with both

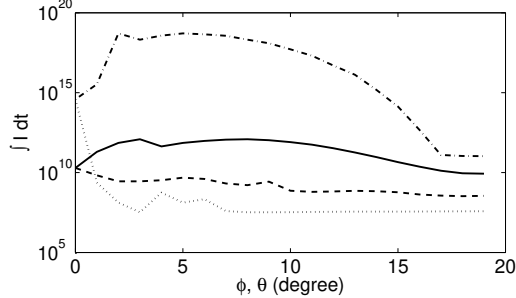


Fig. 4. – The total radiation intensity $\int I(\phi, \theta)d\tau$ for Run C and Run F as a function of the angle (ϕ, θ) . Solid: Run C, $\phi = 0$; Dashed: Run C, $\theta = 0$; Dash-dot: Run F, $\phi = 0$; Dotted: Run F, $\theta = 0$.

ϕ and θ , indicating radiation is strongly collimated in the x direction.

Angular fluence distribution in the θ direction is due to the initial electric field acceleration in z -direction. Since there is no z acceleration after the EM pulse is formed, eventually all the z momentum will be emitted away, which narrows the intensity distribution toward positive x direction. At the same time, however, decoupling of particles from EM pulse in the x direction widens the distribution. Thus, the fluence in the θ direction is always distributed over a finite angle.

In summary, we observed the self-consistent radiation damping effect on the interaction of the EM pulse with electron-positron plasma via a relativistic PIC simulation. Comparison with the non-radiative case showed that radiation damping force decelerates the energetic particle accelerated by the DRPA, and resulting radiation field is strongly linearly polarized within a finite angle from the direction of expansion both in weak and strong magnetic field cases, which may be detectable by γ -ray burst observations or laser experiments as an indication of the DRPA mechanism.

The simulations shown here are still too short to determine the radiation pattern after particles are completely decoupled from EM pulse. Such questions remain as future problems.

* * *

This research is partially supported by NASA Grant No. NAG5-9223 and LLNL contract nos. B528326 and B541027. Authors are also grateful to ILSA, LANL, B. Remington and S. Wilks for useful discussions.

REFERENCES

- [1] LIANG E., and NISHIMURA K., *Phys. Rev. Lett.*, **92** (2004) 175005.
- [2] ZHIDKOV A. *et al.*, *Phys. Rev. Lett.*, **88** (2002) 185002.
- [3] LANDAU L. and LIFSHITS E. M., *The Classical Theory of Fields*, (Pergamon, New York) 1975.
- [4] JACKSON J. D., *Classical Electrodynamics 2nd ed.*, (Wiley, New York) 1975.
- [5] RYBICKI G. B. and LIGHTMAN A. P., *Radiative Processes in Astrophysics*, (Wiley-Interscience, New York) 1979.
- [6] BIRDSALL C. K. and LANGDON A. B., *Plasma Physics via Computer Simulation*, (McGraw-Hill) 1985.